Change of stress regime during geothermal reservoir stimulation

Martin Schoenball[1], Louis Dorbath[2], Emmanuel Gaucher[1], J. Florian Wellmann[3], and Thomas Kohl[1]

[1]Karlsruhe Institute of Technology, Institute of Applied Geosciences, Karlsruhe, Germany, [2]Ecole et Observatoire des Sciences de la Terre, Université de Strasbourg, Strasbourg, France, [3]CSIRO Earth Science and Resource Engineering, Kensington, Western Australia, Australia

Abstract Earthquakes are induced by man-made changes of the stress field by injection or withdrawal of fluids in hydrocarbon production, geothermal exploitation, and wastewater disposal. However, the actual perturbation of the stress field and stress release by injection-induced seismicity remains largely unknown. We provide evidence for currently not understood hydromechanical processes after shut-in of the well. We invert earthquake focal mechanisms from a massive stimulation to invert for stress resolved in time and depth to obtain changes of the stress orientation and magnitude. Prior information about fracture orientations from well logs is taken into account. Comparison with independent stress measures reveals that stresses obtained from inversion of fluid-induced seismicity are highly perturbed and not representative of the initial stress field. The horizontal stresses change by tens of megapascals, turning the stress regime from transitional normal faulting/strike-slip faulting to pure normal faulting. The observed stress changes are attributed to large-scale aseismic deformation.

1. Introduction

The detailed geological and geophysical investigations around massive fluid injection experiments make them a valuable tool for studying mechanisms of seismicity in a relatively well-controlled environment. Hence, deep fluid injection experiments have a long tradition in research on the mechanical properties and the stress state of the Earth's crust [e.g., *Raleigh et al.*, 1976; *Zoback and Harjes*, 1997]. Recently, induced earthquakes in the surrounding of oil, gas and geothermal exploration, exploitation, and deep wastewater injection have caused increased public awareness and the urge for a better understanding of the processes responsible for generating seismicity [*Ellsworth*, 2013]. Besides, natural sequences of seismicity are often connected with deep fluid flow [e.g., *Toda et al.*, 2002; *Hainzl*, 2004]. Here induced seismicity might help us to understand such sequences and the mechanics of earthquakes.

At the exceptionally well-documented enhanced geothermal system in Soultz-sous-Forêts (France) a massive injection with wellhead pressures in the order of 14 MPa was maintained over 6 days during the stimulation treatments of well GPK2 in 2000. Obviously such a massive pressurization accompanied by thousands of recorded microearthquakes tremendously perturbs the local stress field. Yet the actual evolution of the stress field during stimulation remains largely unknown. Based on the analysis of recorded seismicity, *Cornet et al.* [2007] suggest that the stress field rotates with depth. *Cuenot et al.* [2006] obtain different stress regimes from focal mechanism solutions (FMS) at the top and the bottom of the reservoir. Resolved spatially or temporally inversion of focal mechanisms can be used to study the evolution of the stress tensor, e.g., during aftershock sequences [*Michael*, 1987; *Hardebeck and Michael*, 2006; *Hardebeck*, 2012]. Using these methods, *Martínez-Garzón et al.* [2013] traced changes of the stress tensor in time and depth during production in The Geysers geothermal field which correlate with production history.

In this study, we provide observations indicating hydromechanical coupled processes in connection with the shut-in of the well that have been unidentified to date. We use the stress inversion technique, extended with a probabilistic method to consider prior information of fracture planes, to study changes of the stress field in depth and time during and after injection.

2. Observations

The 5000 m deep well GPK2 of the Soultz-sous-Forêts enhanced geothermal system penetrates granite in a horst structure, covered by 1400 m of sediments [*Genter et al.*, 2010]. Fresh water was pumped with rates of
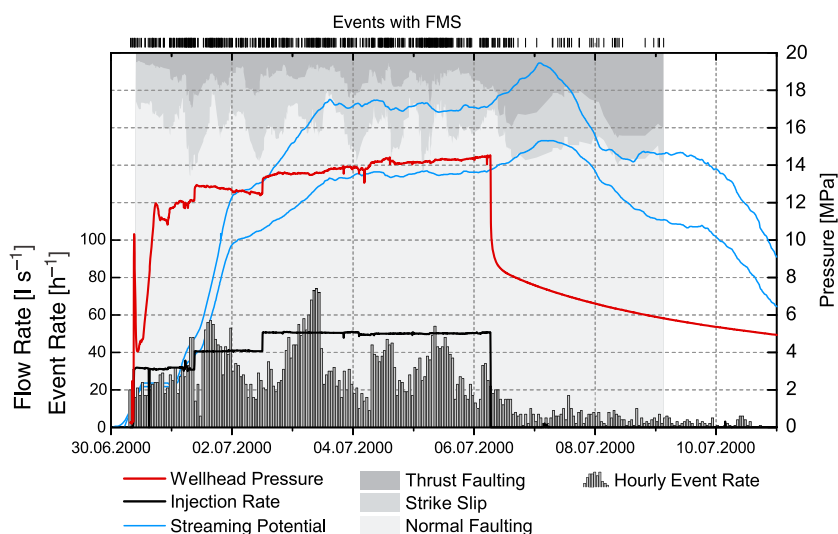
Figure 1. Injection rate (black) and wellhead pressure (red) of the stimulation and hourly seismicity rate (gray bars) of events larger than M_c. The gray shading shows the relative components of faulting style as $\sin^2(\delta_{P,B,T})$ averaged over a sliding window 21 events wide. Blue are measurements of the self-potential made by *Marquis et al.* [2002] and averaged at two sites, drawn in arbitrary units. On the top the occurrence times of events with a focal mechanism are marked by vertical bars.

30 to ls^{-1} for 6 days peaking in 14.5 MPa wellhead pressure. In total, 7215 seismic events with a maximum moment magnitude of 2.5 could be localized. For 715 events with $M_W > 1$ FMS were derived [*Dorbath et al.*, 2009; *Schoenball et al.*, 2012], and these form the basis of our analysis. Figure 1 shows the hydraulic parameters of the stimulation along with the seismic response. Seismicity rate was computed from the full catalog cut down to its completeness magnitude of $M_c = 0.1$ to correct for varying detection thresholds.

Following *Frohlich* [1992] the orientation of the pressure, null, and tension (*P*, *B*, and *T*) axes of the FMS are related by

$$\sin^2 \delta_P + \sin^2 \delta_B + \sin^2 \delta_T = 1, \tag{1}$$

where δ_P, δ_B, and δ_T are the plunges of the *P*, *B*, and *T* axes, respectively. In this definition normal faulting (NF) mechanisms have $\delta_P \approx 90°$, with δ_B and δ_T close to 0°. Strike-slip faulting (SS) corresponds to $\delta_B \approx 90°$, and thrust faulting (TF) corresponds to $\delta_T \approx 90°$ with the other plunges close to zero. The relative proportions of faulting style are defined as $f_{NF} = \sin^2 \delta_P$, $f_{SS} = \sin^2 \delta_B$, and $f_{TF} = \sin^2 \delta_T$ [*Frohlich*, 1992].

We compute an averaged FMS by applying a moving window of 21 events and decompose it into relative proportions of f_{NF}, f_{SS}, and f_{TF}. In agreement with earlier studies on FMS at the Soultz site [*Cuenot et al.*, 2006; *Charléty et al.*, 2007; *Horálek et al.*, 2010], events have predominantly NF mechanisms with an averaged $f_{NF} \approx 79\%$. However, following shut-in of the well, the TF component of the averaged FMS increases significantly from an average of 7% during stimulation to around 15% after shut-in (Figure 1).

Further evidence for these yet not understood mechanisms is given by electric measurements that are independent of the seismic observations. *Marquis et al.* [2002] show that the streaming potential increases significantly just after shut-in (Figure 1). This observation can be interpreted as an enhancement of subsurface fluid flow during this period of the experiment. Peculiarities of postinjection seismicity migration for this stimulation experiment have been noted before [*Dorbath et al.*, 2009]. *Calò et al.* [2011] found an alignment of seismicity in linear structures only during the postinjection period. *Schoenball and Kohl* [2013] demonstrate a clear change of event locations from stationary events during injection to a migration toward the south and upward in the postinjection period. Here static stress transfer might be responsible for progressive triggering, leading to a migration of seismicity locked on large-scale faults [*Schoenball et al.*, 2012]. Together these observations indicate to up to now not recognized hydromechanical processes in connection with shut-in.

The phenomenon of pronounced seismic activity following shut-in has been widely observed at geothermal sites, both during exploration and production phases [*Evans et al.*, 2012], but remains poorly understood.

Models by *Baisch et al.* [2010] and *Goertz-Allmann and Wiemer* [2013] may be able to explain the decrease of the *b* value and the occurrence of the largest events in the postinjection periods, but they cannot explain the observations such as a sudden change of earthquake mechanisms and of the hydraulic regime.

3. Fault Plane Identification

To further investigate the peculiarities observed in connection with shut-in, we conduct stress inversions from FMS to obtain the spatiotemporal evolution of the stress tensor. This technique requires the identification of the fracture plane among the nodal planes as a first step, which is a classical problem of seismology. In the well-defined environment of hydraulic stimulation, additional information is available that helps to identify the fracture plane. *Schoenball et al.* [2012] selected the plane, where the critical pore pressure p_{crit} needed to rupture that plane is minimal, as the fracture plane. *Terakawa et al.* [2012] inverted both nodal planes for the stress tensor individually and chose the plane which yields a stress tensor closer to the stress tensor obtained from independent stress measurements as the fracture plane. However, no structural information of the reservoir was taken into account in both approaches and no confidence measure was estimated.

We propose here a multistep approach to the problem by accounting for available information on fracture geometries derived from well logs. We then consider hydromechanical constraints implied by water injection. The aim is not only to identify the fault plane but to estimate the confidence of the identification as well. Our approach is built up in a way that additional prior information about parameters or measurement errors (for example, for the FMS) can be incorporated, if available.

In the first step, the proximity of a nodal plane orientation to the existing fractures in the reservoir is used to derive a probability distribution for each nodal plane to be a preexisting fracture plane (gray path in Figure 2). We use fractures identified from Ultrasonic Borehole Imager and Formation Micro Imager wellbore imaging of wells GPK2, GPK3, and GPK4 in the depth section of 3000–5000 m (Figure 2a). A weight is computed for all fractures to correct for the sampling bias of inclined fractures along a wellbore wall [*Terzaghi*, 1965]. The correction factor $1/\cos\alpha$ is capped at 10, corresponding to a maximum incidence angle α with the wellbore trajectory of 84°. For each pair composed of a FMS and a randomly picked fracture, we compute the angular distance ⊲(fracture, FMS) of the normal vectors.

We then estimate the probability of each nodal plane to coincide with the selected fracture, considering the error prone determination of the FMS. A von Mises-Fisher [*Fisher*, 1993] probability density function with a mean direction μ of a fracture normal with the concentration parameter κ and the normalization constant $C(\kappa)$ is assigned as

$$\mathrm{PDF}(x) = C(\kappa) \exp(\kappa \mu^T x). \tag{2}$$

We compute the cumulative distribution function (CDF) for a concentration factor $\kappa = 200$, corresponding to a standard deviation of the focal mechanism determination of 4.05° for each direction angle (Figure 2b). We consider the probability of a nodal plane to be the effective fracture plane as proportional to the probability density function (PDF) of the angular distance to the Terzaghi-corrected fracture data set: a nodal plane is more probable to be the actual fracture plane if its orientation is close to the fracture directions determined from wellbore imaging. Based on this consideration, we draw samples from the initial fracture data set and retain them with a probability determined by inverse sampling the corresponding CDF in Figure 2b. Then, the critical pore pressure p_{crit} for each perturbed fracture is computed from the fracture orientation and assuming a stress field and Coulomb criterion as determined by *Cornet et al.* [2007]. Finally, we obtain a distribution of accepted samples p_{crit} for both nodal planes (Figure 2d).

In the second step, we compute a PDF(p_{crit}) for each nodal plane, taking into account the error of FMS determination (red path in Figure 2). Since the fluid pressure decreases with distance from the injection well, the probability to trigger a fracture with a higher critical pore pressure p_{crit} is, in general, smaller compared to a lower p_{crit}. To account for this effect, we multiply the PDF(p_{crit}) for each nodal plane with a factor 1 for critical pore pressures of $p_{crit} = 0$ and linearly decreasing to 0 for $p_{crit} = 20$ MPa (Figure 2c). All planes with critical pore pressures of $p_{crit} > 20$ MPa are considered unrealistic given the maximum sustained injection wellhead pressure of 14.5 MPa and allowing for uncertainty and spatial variation in the determination of the Mohr-Coulomb criterion for reactivation of preexisting fractures (Figure 2e). This very simplistic model for the pressure distribution was chosen on purpose over other analytical models in order to reduce a bias due
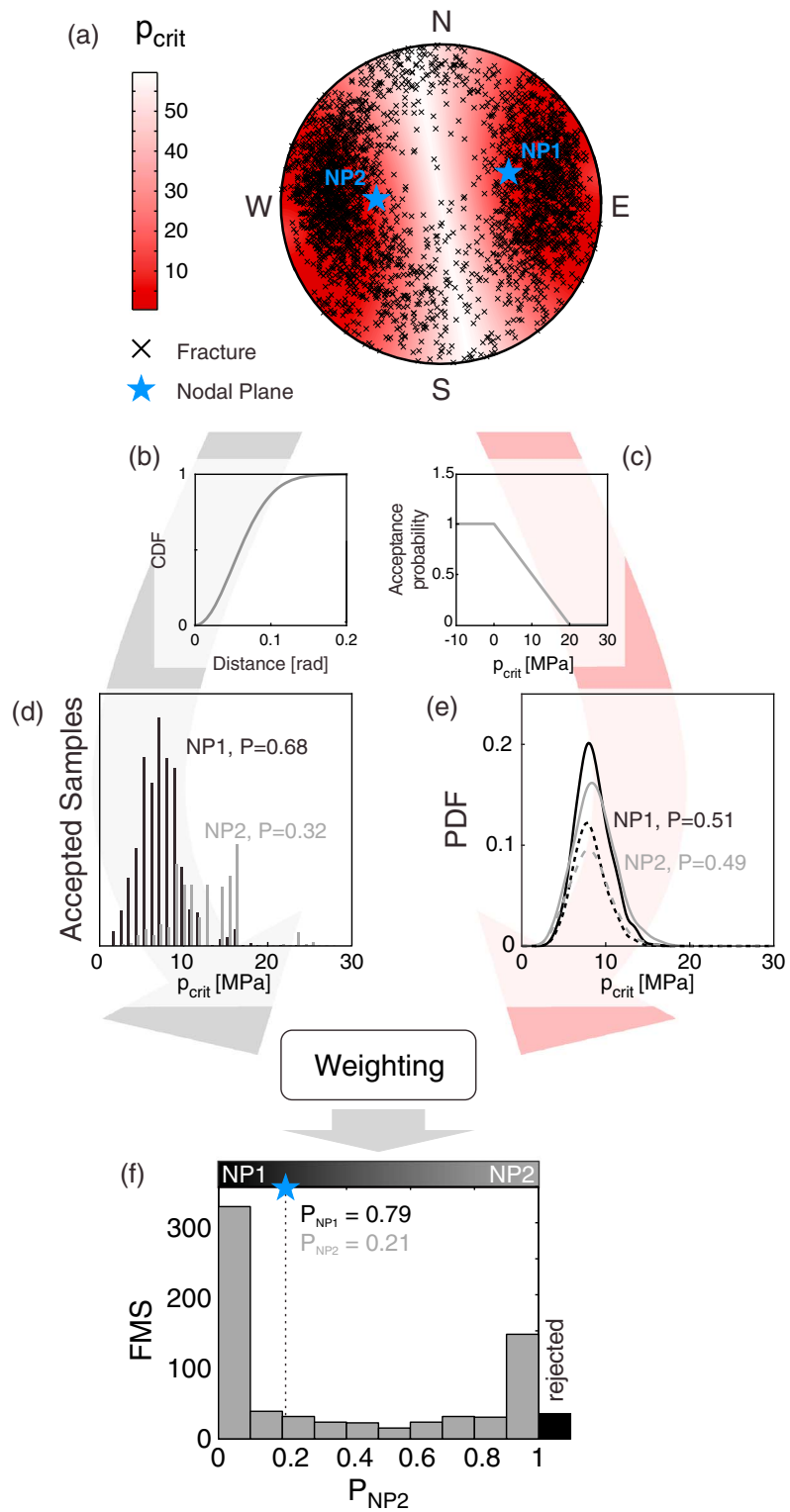
Figure 2. Quantification of the probability to determine the fracture plane for one sample FMS. (a) Normal vectors of fractures identified on wellbore logs and of the two nodal planes of the FMS on lower hemisphere projection. The red shading corresponds to p_{crit}. (b) Cumulative distribution function of the von Mises-Fisher distribution for $\kappa = 200$. (c) Probability to retain a nodal plane as function of pore pressure in the reservoir. (d) Distribution of p_{crit} for accepted samples for NP1 and NP2. (e) Distribution of critical pore pressures for nodal planes with added von Mises-Fisher distributed errors (solid) and multiplied with the pore pressure probability (dashed) for the example FMS. (f) Probability distribution of the fracture plane to be either NP1 or NP2 for all FMS.

to a particular model requiring further assumptions on the hydraulic flow in the reservoir as either porous matrix flow or fracture flow or mixtures. Yet it covers the first-order observation of pore pressure decrease with radial distance from the injection well. In a final step, the normalized marginals for all samples of the nodal planes are determined, yielding relative probabilities of each nodal plane to be the fracture plane.

Out of the catalog of 715 FMS the fault plane could be determined for 680 FMS and 467 fault planes could be determined with > 90% confidence (Figure 2f). The fault planes of 35 FMS could not be determined by our model, as p_{crit} > 20 MPa for both nodal planes; hence, they were rejected by the pressure distribution factor. The mechanics of these events remain unclear, as they would require unusually low friction angles to be triggered by the pore fluid pressure perturbation of the hydraulic stimulation when assuming a Coulomb criterion. We still included them in the further analysis, since they were measured and might hold valuable information. For these events we assumed a 50% probability for each nodal plane.

4. Stress Inversions and Results

In order to image the stress in the Soultz reservoir, we use the stress inversion code Spatial And Temporal Stress Inversion (SATSI) [*Hardebeck and Michael*, 2006]. This code enables damped inversion when spatially and/or temporally resolved inversions are performed, taking inversion results of neighboring bins into account. This procedure enables a reduction of the complexity of the resulting stress model in order to minimize artifacts due to poor data coverage or outliers [*Hardebeck and Michael*, 2006].

While SATSI is capable of 4-D inversion, we restrict our analysis to problems of lower dimensionality. In doing so, we implicitly assume a stress field constant along the neglected dimensions. Inversions of the 1-D temporal evolution of the stress tensor orientation showed an apparent rotation of the stress tensor during the postinjection period. However, closer investigation revealed that this might be a geometrical effect, as events migrate upward during this phase of the experiment [*Schoenball and Kohl*, 2013], and the observed stress rotation reflects spatial stress changes rather than temporal stress changes. Also, postinjection events have a higher TF component (Figure 1) which might be related to the observed rotation of the stress tensor following shut-in. From these observations we conclude that the inferred rotation of the stress tensor is either related to (a) the location of seismicity in depth, which might be due to changing geology. In fact, the shallow section of the reservoir (down to approximately 4800 m) is different to the one in the deep section [*Hooijkaas et al.*, 2006]. Or (b) temporal changes of the stress tensor are caused by hydromechanical couplings related to the transition from coinjection to postinjection phases of the experiment.

For further analysis we bin the catalog of FMS in 20 bins each in time and depth, implicitly assuming no variation of the stress field in horizontal directions. Due to the damping used during inversion even bins with very few events still yield consistent results. To test the robustness and estimate confidence intervals of our results we perform 2000 inversions each on a data set perturbed as follows. For each FMS, we randomly draw the fault plane according to the previously determined probability distribution of the nodal planes. In order to capture the location uncertainty, we add normally distributed errors with a standard deviation of 50 m to the depth coordinate and von Mises-Fisher distributed errors with $\kappa = 200$, as described above, to the P, B, and T axes of the nodal plane. To test the robustness toward removal of data points, we perform 100 jackknife tests for each of these data sets by randomly removing 10% of the FMS from the data set that is used for the inversions. The damping parameter e for the inversion is retrieved from the trade-off between the complexity of the resulting model versus the misfit of the model with measured data (Figure 3a). A slightly overdamped value of $e = 0.8$ was chosen. Stress inversion yields the nonisotropic parts of the principal stresses σ_1, σ_2, and σ_3 and therefore also the shape factor

$$\phi = \frac{\sigma_2 - \sigma_3}{\sigma_1 - \sigma_3}.$$

(3)

The isotropic part of the stress tensor (which includes the pore pressure perturbation due to fluid injection) and hence stress magnitudes cannot be determined from stress inversions without further assumptions.

We find a normal faulting regime with σ_1 close to vertical for the entire experiment. Taking the stress magnitudes of the unperturbed stress field as determined by *Cornet et al.* [2007], we would expect $\phi \approx 1$. The results of the stress inversion, however, show very different values. In Figure 3d, we show ϕ averaged
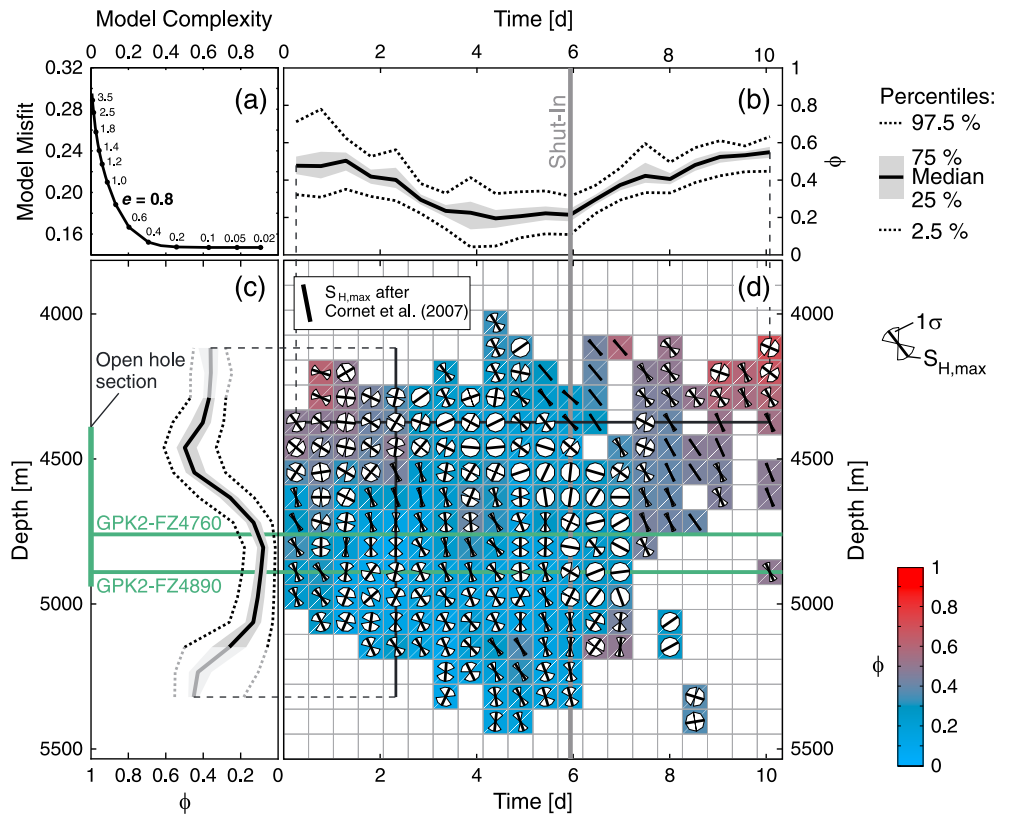
Figure 3. Two-dimensional stress inversion in time-depth space. (a) The trade-off between the complexity of the model, the data misfit, and the damping parameter e. (b and c) Sections of the results in time and depth, respectively, showing median of ϕ, its variation by first and third quartiles (shading), and range of the 95% confidence interval (dashed). (d) Color-coded ϕ; the position of sections in Figures 3b and 3c is indicated with black lines. The symbols in each bin indicate the direction of S_{Hmax} and its 1σ variation. Bins that were successfully determined in less than 25% of the inversions (representing single events with large perturbations of depth) are not drawn. The gray line marks the time of shut-in; green lines highlight two major fracture zones with significant fluid inflow.

from all inversions and the orientation of the maximum subhorizontal stress S_{Hmax}. Figures 3b and 3c show the distribution of ϕ in sections of the 2-D inversion (location of sections indicated with black lines in Figure 3d). Starting from the open hole section of the well GPK2 between 4390 m and 4940 m depth, a front
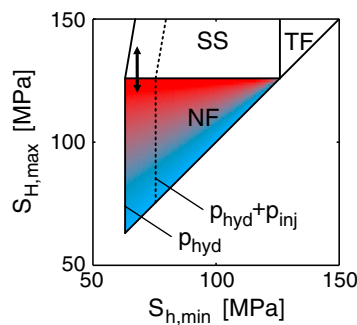

Figure 4. Lower part of stress polygon after *Zoback et al.* [2003] at 5000 m depth with shading for ϕ. The range of the unperturbed stress field (double arrow) and coefficient of friction $\mu = 1.0$ are taken from *Cornet et al.* [2007]. Dashed lines mark the change of allowed stress states for a pore pressure increase by 15 MPa.

of very low ϕ propagates both upward and downward, delineating the propagation of induced seismicity. Initially, shallower parts of the reservoir show a high value of ϕ but do not reach the expected order for the unperturbed rock of $\phi \approx 1$, since their stress field is already perturbed by seismicity. A minimum of ϕ is reached after 3 days in the depth where the open hole section of the well is cut by two major inflow zones as identified by *Sausse et al.* [2010]. Here ϕ is reduced to almost zero, which translates to $\sigma_2 \approx \sigma_3$ or applied to the NF stress field in Soultz that $S_{Hmax} \approx S_{hmin}$. Assuming that the vertical stress is equivalent to the overburden, we can consider it to be constant throughout the stimulation. A change in ϕ can therefore be attributed to an increase of S_{hmin} or a decrease of S_{Hmax} or both. Either way, the stress changes required to change ϕ as determined are in the order of tens of megapascals, as shown by the stress polygon after *Zoback et al.* [2003] in Figure 4.

The edges of the stimulated region show only a small perturbation of the stress field, whereas the strongest stress perturbations are confined to the seismically active volume. Analyzing induced seismicity in The Geysers hydrogeothermal field, *Martínez-Garzón et al.* [2013] find similar reductions of ϕ within the reservoir and increasing values outside. This behavior was predicted for production scenarios considering poroelastic coupling by *Segall and Fitzgerald* [1998].

Following shut-in, ϕ increases gradually. This is mostly a geometrical effect, as after shut-in seismicity migrates into areas which were not active previously and therefore contain a largely unperturbed stress field, as observed at the beginning of the injection in the shallow part. Seismic activity in the previously active volume practically stops.

Also shown in Figure 3d is the orientation of S_{Hmax} and its standard deviation for each bin. Areas showing low values of ϕ typically show a strong variation of the S_{Hmax} orientation. This behavior is expected as even small stress perturbations can lead to significant stress tensor rotations when $S_{Hmax} \approx S_{hmin}$. Our findings of a strong reduction of horizontal shear stresses are supported by the fact that it is difficult to distinguish between NF (σ_1 vertical) and SS (σ_2 vertical) stress regimes from stress measurements based on borehole data, since $S_v \approx S_{Hmax}$ [*Cornet et al.*, 2007]. Yet seismicity is predominantly of NF type. A reduction of S_{Hmax} changes the stress regime from a transitional NF/SS regime ($S_v \approx S_{Hmax}$) to a pure NF regime with $S_v > S_{Hmax}$; hence, only NF mechanisms are observed.

5. Conclusions

New evidence is presented for the complexity of hydromechanical couplings occurring after termination of massive hydraulic stimulation treatments. In a detailed investigation, we determined a changing behavior of seismicity showing an upward migration and a change in mechanism during and after the stimulation experiment. This observation can partly be related to triggering by static stress transfer [*Schoenball et al.*, 2012]. The observed change of earthquake mechanism and the enhanced fluid flow seen on measurements of the streaming potential [*Marquis et al.*, 2002] have not been explained previously.

Our analysis is based on stress inversions in which potential fracture planes were identified with a probabilistic method considering 715 FMS and additional structural and independent stress data as prior information. Random perturbation of the initial data set in its uncertainty domain allowed to quantify uncertainties in the stress distributions in time and depth. Derived spatiotemporal stress changes during massive hydraulic stimulation revealed a strong reduction of the maximum subhorizontal stress, changing the stress regime from transitional NF/SS to a pure NF regime. As a result, almost only pure NF earthquakes are observed during the stimulation. Similar results were obtained by *Martínez-Garzón et al.* [2013] for The Geysers geothermal reservoir in production conditions where a NF/SS stress regime was determined in an otherwise SS-dominated region. The observed change in earthquake mechanisms following shut-in can be explained as a result of the migration of seismicity into previously seismically inactive areas sampling a relatively unperturbed stress field.

Calò et al. [2011] obtained a large low-velocity zone centered on the microseismicity cloud of the GPK2 stimulation from 4-D tomography which was interpreted as a zone of large-scale release of stress in the order of several tens of megapascals. These complementary observations agree well with our findings. The comparison of our results with an analysis of the coseismic static stress transfer [*Schoenball et al.*, 2012] reveals a large discrepancy with much more stress released than seismically observed. In line with the analysis of *Calò et al.* [2011] and indirect observations of large-scale creep at previous stimulations in Soultz [*Cornet et al.*, 1997; *Bourouis and Bernard*, 2007], the stress discrepancy is strong evidence for large-scale aseismic deformations occurring during massive hydraulic stimulation. If we succeed in triggering specifically these aseismic processes during stimulation, we might hold the key to mitigate induced seismicity while meeting our goals for reservoir enhancement.

Furthermore, we propose that stress orientations gained from inversion of focal mechanisms of fluid-induced events are not representative of the initial virgin stress field. This interpretation is obvious when comparing results of inversions with independent stress measurements obtained from wellbore logs. First, they sample the perturbed stress field and second, due to the strong reduction of S_{Hmax} during stimulation, small (local) perturbations are sufficient to change the stress orientation significantly.

References

Baisch, S., R. Vörös, E. Rothert, H. Stang, R. Jung, and R. Schellschmidt (2010), A numerical model for fluid injection induced seismicity at Soultz-sous-Forêts, *Int. J. Rock Mech. Min. Sci.*, *47*(3), 405–413, doi:10.1016/j.ijrmms.2009.10.001.

Bourouis, S., and P. Bernard (2007), Evidence for coupled seismic and aseismic fault slip during water injection in the geothermal site of Soultz (France), and implications for seismogenic transients, *Geophys. J. Int.*, *169*(2), 723–732, doi:10.1111/j.1365-246X.2006.03325.x.

Calò, M., C. Dorbath, F. H. Cornet, and N. Cuenot (2011), Large-scale aseismic motion identified through 4-D P-wave tomography, *Geophys. J. Int.*, *186*(3), 1295–1314, doi:10.1111/j.1365-246X.2011.05108.x.

Charléty, J., N. Cuenot, L. Dorbath, C. Dorbath, H. Haessler, and M. Frogneux (2007), Large earthquakes during hydraulic stimulations at the geothermal site of Soultz-sous-Forêts, *Int. J. Rock Mech. Min.*, *44*(8), 1091–1105, doi:10.1016/j.ijrmms.2007.06.003.

Cornet, F. H., J. Helm, H. Poitrenaud, and A. Etchecopar (1997), Seismic and aseismic slips induced by large-scale fluid injections, *Pure Appl. Geophys.*, *150*, 563–585, doi:10.1007/978-3-0348-8814-1_12.

Cornet, F., T. Bérard, and S. Bourouis (2007), How close to failure is a granite rock mass at a 5km depth, *Int. J. Rock Mech. Min.*, *44*(1), 47–66, doi:10.1016/j.ijrmms.2006.04.008.

Cuenot, N., J. Charléty, L. Dorbath, and H. Haessler (2006), Faulting mechanisms and stress regime at the European HDR site of Soultz-sous-Forêts, France, *Geothermics*, *35*(5–6), 561–575, doi:10.1016/j.geothermics.2006.11.007.

Dorbath, L., N. Cuenot, A. Genter, and M. Frogneux (2009), Seismic response of the fractured and faulted granite of Soultz-sous-Forêts (France) to 5 km deep massive water injections, *Geophys. J. Int.*, *177*(2), 653–675, doi:10.1111/j.1365-246X.2009.04030.x.

Ellsworth, W. L. (2013), Injection-induced earthquakes, *Science*, *341*(6142), 1225,942, doi:10.1126/science.1225942.

Evans, K., A. Zappone, T. Kraft, N. Deichmann, and F. Moia (2012), A survey of the induced seismic responses to fluid injection in geothermal and CO_2 reservoirs in Europe, *Geothermics*, *41*, 30–54, doi:10.1016/j.geothermics.2011.08.002.

Fisher, N. I. (1993), *Statistical Analysis of Circular Data*, Cambridge Univ. Press, Cambridge, U.K.

Frohlich, C. (1992), Triangle diagrams: Ternary graphs to display similarity and diversity of earthquake focal mechanisms, *Phys. Earth Planet. Inter.*, *75*(1–3), 193–198, doi:10.1016/0031-9201(92)90130-n.

Genter, A., K. Evans, N. Cuenot, D. Fritsch, and B. Sanjuan (2010), Contribution of the exploration of deep crystalline fractured reservoir of Soultz to the knowledge of enhanced geothermal systems (EGS), *C. R. Geosci.*, *342*(7–8), 502–516, doi:10.1016/j.crte.2010.01.006.

Goertz-Allmann, B. P., and S. Wiemer (2013), Geomechanical modeling of induced seismicity source parameters and implications for seismic hazard assessment, *Geophysics*, *78*(1), KS25–KS39, doi:10.1190/geo2012-0102.1.

Hainzl, S. (2004), Seismicity patterns of earthquake swarms due to fluid intrusion and stress triggering, *Geophys. J. Int.*, *159*(3), 1090–1096, doi:10.1111/j.1365-246X.2004.02463.x.

Hardebeck, J. L. (2012), Coseismic and postseismic stress rotations due to great subduction zone earthquakes, *Geophys. Res. Lett.*, *39*, L21313, doi:10.1029/2012GL053438.

Hardebeck, J. L., and A. J. Michael (2006), Damped regional-scale stress inversions: Methodology and examples for southern California and the Coalinga aftershock sequence, *J. Geophys. Res.*, *111*, B11310, doi:10.1029/2005JB004144.

Hooijkaas, G. R., A. Genter, and C. Dezayes (2006), Deep-seated geology of the granite intrusions at the Soultz EGS site based on data from 5km-deep boreholes, *Geothermics*, *35*(5–6), 484–506, doi:10.1016/j.geothermics.2006.03.003.

Horálek, J., Z. Jechumtálová, L. Dorbath, and J. Šílený (2010), Source mechanisms of micro-earthquakes induced in a fluid injection experiment at the HDR site Soultz-sous-Forêts (Alsace) in 2003 and their temporal and spatial variations, *Geophys. J. Int.*, *181*(3), 1547–1565, doi:10.1111/j.1365-246X.2010.04506.x.

Marquis, G., M. Darnet, P. Sailhac, A. K. Singh, and A. Gérard (2002), Surface electric variations induced by deep hydraulic stimulation: An example from the Soultz HDR site, *Geophys. Res. Lett.*, *29*(14), 1662, doi:10.1029/2002GL015046.

Martínez-Garzón, P., M. Bohnhoff, G. Kwiatek, and G. Dresen (2013), Stress tensor changes related to fluid injection at The Geysers geothermal field, California, *Geophys. Res. Lett.*, *40*, 2596–2601, doi:10.1002/grl.50438.

Michael, A. J. (1987), Stress rotation during the Coalinga aftershock sequence, *J. Geophys. Res.*, *92*(B8), 7963–7979, doi:10.1029/JB092iB08p07963.

Raleigh, C. B., J. H. Healy, and J. D. Bredehoeft (1976), An experiment in earthquake control at Rangely, Colorado, *Science*, *191*(4233), 1230–1237, doi:10.1126/science.191.4233.1230.

Sausse, J., C. Dezayes, L. Dorbath, A. Genter, and J. Place (2010), 3D model of fracture zones at Soultz-sous-Forêts based on geological data, image logs, induced microseismicity and vertical seismic profiles, *C. R. Geosci.*, *342*(7–8), 531–545, doi:10.1016/j.crte.2010.01.011.

Schoenball, M., and T. Kohl (2013), The peculiar shut-in behavior of the well GPK2 at Soultz-sous-Forêts, *GRC Trans.*, *37*, 217–220.

Schoenball, M., C. Baujard, T. Kohl, and L. Dorbath (2012), The role of triggering by static stress transfer during geothermal reservoir stimulation, *J. Geophys. Res.*, *117*, B09307, doi:10.1029/2012jb009304.

Segall, P., and S. D. Fitzgerald (1998), A note on induced stress changes in hydrocarbon and geothermal reservoirs, *Tectonophysics*, *289*(1–3), 117–128, doi:10.1016/s0040-1951(97)00311-9.

Terakawa, T., S. A. Miller, and N. Deichmann (2012), High fluid pressure and triggered earthquakes in the enhanced geothermal system in Basel, Switzerland, *J. Geophys. Res.*, *117*, B07305, doi:10.1029/2011JB008980.

Terzaghi, R. (1965), Sources of error in joint surveys, *Geotechnique*, *15*(3), 287–304.

Toda, S., R. S. Stein, and T. Sagiya (2002), Evidence from the AD 2000 Izu islands earthquake swarm that stressing rate governs seismicity, *Nature*, *419*(6902), 58–61, doi:10.1038/nature00997.

Zoback, M., and H.-P. P. Harjes (1997), Injection-induced earthquakes and the crustal stress at 9 km depth at the KTB deep drilling site, Germany, *J. Geophys. Res.*, *102*, 18,477–18,491, doi:10.1029/96JB02814.

Zoback, M. D., C. A. Barton, M. Brudy, D. A. Castillo, T. Finkbeiner, B. R. Grollimund, D. B. Moos, P. Peska, C. D. Ward, and D. J. Wiprut (2003), Determination of stress orientation and magnitude in deep wells, *Int. J. Rock Mech. Min.*, *40*(7–8), 1049–1076, doi:10.1016/j.ijrmms.2003.07.001.